Robotics and Computer Integrated Manufacturing 59 (2019) 385–393

Contents lists available at ScienceDirect

Robotics and Computer Integrated Manufacturing

journal homepage: www.elsevier.com/locate/rcim

Increasing stability in robotic GTA-based additive manufacturing through optical measurement and feedback control☆

Jun Xiong*, Guangchao Liu, Yupeng Pi

Key Laboratory of Advanced Technologies of Materials, Ministry of Education, School of Materials Science and Engineering, Southwest Jiaotong University, Chengdu 610031, China

ARTICLE INFO

Keywords:
Additive manufacturing
Robotic GTA
Optical measurement
Process stability
Low-carbon steel

ABSTRACT

Additive manufacturing employing Gas Tungsten Arc (GTA) as the heat source is capable of fabricating fully dense metal components layer upon layer. However, this process is sensitive to various disturbances and needs on-line detection and adjustments. In this work, a visual sensor, comprising a camera and composite filters, is developed for automatically real-time sensing of the fabrication process. The aim is to keep stable manufacture, and the deviations of the deposited height are compensated by designing an integral separation PID controller to adjust the wire feed speed in the next layer. The optical measurement technique and the controller are estimated via building multi-layer single-pass walls. The results show that the process stability in GTA-based additive manufacturing is well controlled when the designed visual sensor and the proposed closed-loop controller are applied.

1. Introduction

Wire plus Arc Additive Manufacturing (WAAM) is an innovative technique that enables the manufacture of complicated, near-net shape parts layer upon layer, using electric arc as the heat power and wire as the adding material [1,2]. In comparison to laser plus powder additive manufacturing, WAAM is gaining more attention thanks to significant merits of lower equipment cost, higher material utilization, and less contamination issues [3–5]. In WAAM, the metal wire is melted by the arc heat source and droplets are dropped into the molten pool to form continuous beads. This technique is suitable to build large-size metal components due to its high deposition rates [6]. Generally, the motion in WAAM is usually provided by a robotic system to fabricate complex parts. For instance, Kazanas et al. [7] proposed a positional deposition approach to produce geometrical features using robotic WAAM. It was found that the torch controlled by the robot could be inclined to the wall direction to produce complex features. As described in Ding et al. [8], a Medial Axis Transformation (MAT) methodology was proposed to generate deposition path for robotic WAAM, indicating that the MAT-based path patterns showed excellent performance in terms of gap-free cross-sections. In recent years, studies concerning WAAM have been extensively explored, e.g. slicing process for three-dimensional models [8,9], microstructure and mechanical performance of deposited parts [10,11], and heat characteristics as well as stress distribution [12,13].

As addressed in Li et al. [14], the common heat sources in WAAM are Gas Metal Arc (GMA), Gas Tungsten Arc (GTA), and Plasma Arc (PA). Low-cost investment of the device makes GTA the most widely applied technique in the industry field. The separation of heat input and filling wire in GTA-based additive manufacturing is beneficial to controlling the process energy input, thus ensuring fabrication of metal parts with excellent microstructure and mechanical properties [15].

During robotic GTA-based additive manufacturing, the arc is directly struck between the tungsten tip and base metal. As one layer is performed, the GTA torch is made a lifting with a predefined layer height along the deposition height direction. Nevertheless, the fabricated layer height is not always the same as the expected slicing height calculated from a three-dimensional model. This is because process parameters including the arc current, arc length, and wire feed speed may fluctuate easily during the deposition process, producing variable layer geometries. Furthermore, heat conduction state at different positions, substrate size, inter-layer temperature, and previous layer geometry greatly affect the current layer size. After multi-layer depositions, the arc length or the distance between the tungsten and top layer will change markedly. It is known that the arc length approximately ranging from 3 to 7 mm can contribute to maintaining the process stability in GTA.

☆ Conflicts of interest: We declare that we do not have any commercial or associative interest that represents a conflict of interest in connection with the work submitted.

* Corresponding author.
E-mail address: xiongjun@home.swjtu.edu.cn (J. Xiong).

https://doi.org/10.1016/j.rcim.2019.05.012
Received 17 May 2018; Received in revised form 14 May 2019; Accepted 16 May 2019
Available online 20 May 2019

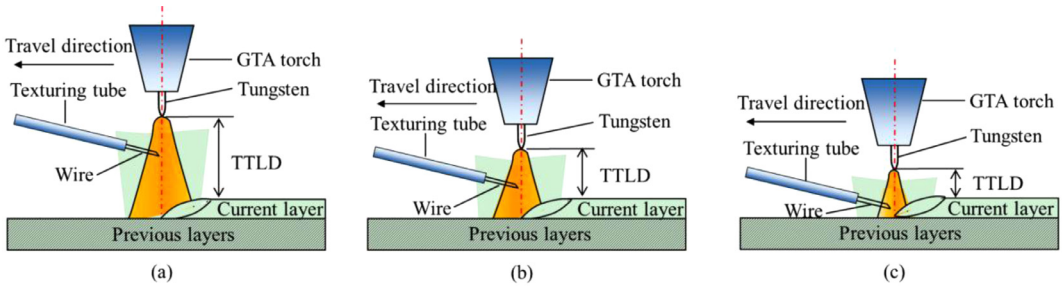

Fig. 1. Schematic diagram of wire direction passing through the arc when the tungsten to top layer distance changes. (a) Long TTLD. (b) Suitable TTLD. (c) Short TTLD.

Fig. 1 presents a schematic diagram of the wire direction passing through the arc in GTA-based additive manufacturing as the Tungsten to Top Layer Distance (TTLD) changes. As shown in Fig. 1(a), provided that the arc length or the TTLD is too long, the arc energy disperses due to a large arc volume. The wire feeding direction passes through the upper of the arc, and the wire is melted slowly and the droplet presents globular transfer, seriously decreasing the process stability and even preventing the proceeding of GTA-based additive manufacturing. As presented in Fig. 1(c), if the arc length or the TTLD is too short, the texturing tube and wire will contact the substrate or the previous layers, leading to difficulties for smooth wire feeding. Consequently, on-line detection and manipulation of the arc length or the TTLD are critical issues in GTA-based additive manufacturing for improving the process stability.

In recent years, some measures have been adopted to monitor the WAAM process. For example, Yang et al. [3] used an advanced infrared thermography to capture the surface temperatures of multi-layer single-pass components built in GMA-based additive manufacturing. However, the expensive cost of this sensing approach will limit its further application, and infrared sensing can only supply temperature data for an operator and lacks the capacity of automatic data analysis. In Bonaccorso et al. [16], the torch height from layer surface in GTA-based additive manufacturing was monitored by means of electrical parameters sensing based on the linear relationship between arc voltage and arc length. Nevertheless, the arc voltage signal is sensitive to experimental conditions, and the resolution ratio of arc voltage relative to arc length is not high enough. To deal with this issue, a promising approach is to utilize optical measurement techniques which have been demonstrated to be powerful tools to monitor arc or laser-based process due to merits of low-cost device and visualized information [17,18]. To the best knowledge of the authors, publications related to on-line monitoring and process control are mainly focused on laser-based additive manufacturing. For instance, optical measurements and closed-loop control techniques were applied to increase the process stability in laser metal wire additive manufacturing [19], and the deposition height was monitored and controlled by a three-dimensional scanning system and an iterative learning control algorithm [20]. In Tang and Landers [21], a laser metal fabrication height control method was proposed, in which the height controller employed a particle swarm optimization algorithm to evaluate model parameters from determined temperatures and track height profiles between deposited layers. It was indicated that this methodology could produce more consistent deposition height.

To our knowledge, visual sensing has been utilized in arc-based welding process for extensive applications, such as seam tracking [17,22], weld pool determination [23,24], and weld pool surface reconstruction [25,26]. For instance, He et al. [22] used a laser vision sensor to detect the weld seam profile and extract feature points in multi-pass welding for thick plates. As reported in Xiong and Zou [23], a novel active vision sensing technique was proposed to monitor the back penetration for thin sheet aluminum alloy in pulsed GMA suspension welding, and a fuzzy controller was applied for back width control. Liu and Zhang [26] employed a laser generator capable of projecting a dot matrix structured light pattern to measure the weld pool surface characterized by its length, width, and convexity.

By contrast, only several studies have been reported in WAAM. As described in Doumanidis and Kwak [27], a laser vision system was applied to detect the deposition height and width in GMA-based additive manufacturing, and a multi-variable adaptive controller was designed for geometry control of thin-walled parts. However, the laser line projecting on the solidified layers was 25.4 mm away from the wire electrode, producing a large detection lag of the sensing system and causing excessive overshoot of the control system. Comas et al. [28] used a passive imaging system to measure layer geometry in PA additive manufacturing process, and corresponding camera calibration algorithms were studied. Xiong and Zhang [29] designed two passive vision sensors to monitor the molten pool tail of deposited layers in GMA-based additive manufacturing, and the sensor calibration and continuous detection were validated by means of depositing thin walls. Further, a segmented neuron self-learning controller was used for the layer width control in GMA-based additive manufacturing [30], and the on-line control of the deposition height was also realized based on an adaptive controller [31], demonstrating that the application of the closed-loop controller could produce a more consistent layer width and a more precise deposition height. For GTA-based additive manufacturing, a visual sensor was utilized to detect the arc length when building thin-walled parts of aluminum alloy [32,33]. In their work, to increase the process stability, the torch height was adjusted to maintain a constant arc length. Nevertheless, the control aim in this research is different from the concept of the additive manufacturing process in which the deposited layer height should be equal to the torch step height designed in the slicing process.

Considering the poor process stability in GTA-based additive manufacturing, corresponding detection and control strategies must be developed. In this study, a visual sensor is designed to monitor the GTA tungsten tip to the top surface distance, and a controller is developed to automatically increase the process stability. Finally, thin-walled parts are chosen to validate the effectiveness of the optical measurement and feedback control system.

2. Methods

2.1. Experimental setup

As shown in Fig. 2, the GTA-based additive manufacturing system is mainly composed of a MOTOMAN-MH24 robot, a MagicWave 3000 Job G/F welding power supply, a KD4010 wire feeding equipment, a visual sensor, a control box, a personal computer, and a platform. The wire feeder had a high response speed to the change in feeding rate signal. The visual sensor, installed on the GTA torch by a specially designed fixture, was utilized to detect the positions of the tungsten tip and deposited layers. The personal computer was the central of the sensing and deposition system. It is capable of realizing the following functions: adjusting the process parameters, displaying images captured from the visual sensor, and providing a human-machine interface designed for

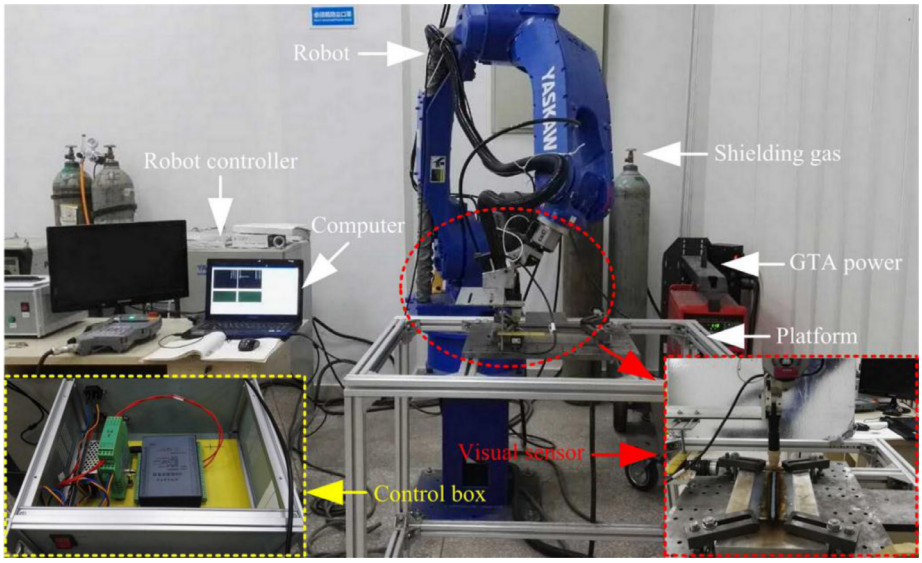

Fig. 2. Experimental setup of robotic GTA-based additive manufacturing system.

control operation. The adjustments of arc current and wire feed speed were carried out by a data acquisition card and an external control device ROB5000. The data acquisition card was integrated in the control box, as depicted with the yellow short dash line in Fig. 2. It was connected to the personal computer with a Universal Serial Bus (USB) and is able to output analog signals with the amplitude of 0–10 V to the ROB5000 for process parameters regulation.

The GTA torch was fixed on the six-axis of the robot, and its movement was realized by the robot controller. For a higher deposition rate, front feeding, in which the wire feeding was set in front of the arc along the deposition path. The angle between the tungsten and the wire feed orientation was about 65°. The electric arc was ignited between the tungsten and the base metal. Q235B low-carbon steel was employed as the substrate with dimensions of 180 mm × 80 mm × 5 mm. The adding material was H08Mn2Si with a diameter of 1.2 mm. The chemical compositions of the wire and the substrate can be referred to a previous publication, as described in Xiong et al. [34]. 99.99% Ar atmosphere with a gas flow rate of 15 L/min was used as the shielding gas to protect the molten pool.

Thin-walled components were fabricated by the GTA-based additive manufacturing experimental system. It is worth noting that if no particular statements, the arc current was kept at 150 A with direct current mode, and the travel speed was 4 mm/s. During the deposition process, as a layer was completed, the arc was turned off and the GTA torch was increased by a given value along the height direction. An idle time of 60 s was carried out between every two continuous layers, preventing poor forming appearance of parts due to molten pool overflow caused by high inter-layer temperature. Then, the arc was ignited and a new layer was deposited. The travel paths between adjacent layers were inverse, which was achieved by converting the robot pose.

2.2. Visual sensor design and image processing

Based on the basic idea of additive manufacturing, the deposited layer height must be equal to the slicing height of a three-dimensional model. Due to disturbances of fluctuations of process parameters and heat accumulation, the deposited layer height is not always identical with the torch step height. However, the layer height is not easy to be determined directly, owing to the particular operative conditions. The TTLD can give indirect information of material deposited (total height). Thus, the visual sensor, consisting of a camera, a lens, a dimmer glass, and a narrow-band filter, is designed to monitor the TTLD, as shown in Fig. 3. Provided that the TTLD is kept consistent in GTA-based additive manufacturing, the process can be regarded as stable.

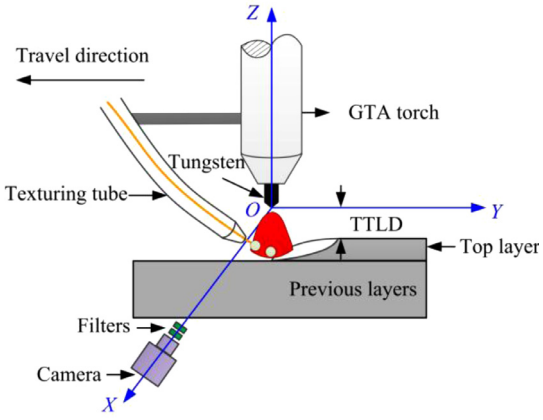

Fig. 3. Schematic diagram of visual sensor system.

As presented in Fig. 3, the central axis of the camera is along the *X*-axis. Namely, the visual sensor is fixed opposite the GTA torch. In this research, the robot was responsible for the movement of the torch, and the platform was stationary during the deposition process. Measuring the vertical distance from the tungsten tip to the top edge of the current layer can represent the accurate accumulation error between the deposited and expected total height. As presented in Fig. 3, provided that the visual sensor is fixed behind the GTA torch in the *YOZ*-plane, it can also capture the tungsten tip as well as the width and top edge of the deposited layer. However, the top edge of the current layer is hard to be extracted from the image by image processing algorithms. Moreover, the camera calibration process becomes difficult due to the fact that only one camera cannot easily obtain the depth information in the image.

The MER-125-30UM-L digital camera can capture gray scale images with 1292 × 964 pixels, and its sampling frequency was 30 fps. The focal length of the lens was 35 mm, and the lens plane to the tungsten distance was about 130 mm. The dimmer glass with a transmissivity of 2% was installed in front of the camera to weaken strong radiation lights from the arc. Under this circumstance, with the appropriate aperture of the camera, an unsaturated molten pool image was obtained. Because deposited layers at high temperature mainly radiate red lights, the narrow-band filter with a center wavelength of 685 nm was fixed on the camera to capture clear shapes of the molten pool and

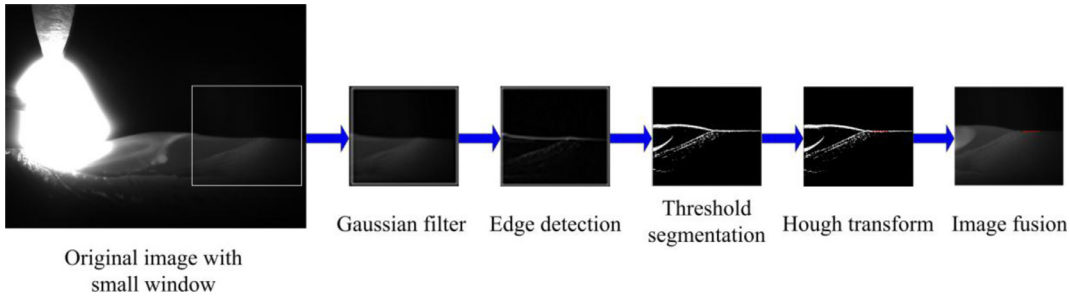

Fig. 4. Procedure of image processing for determining TTLD in GTA-based additive manufacturing.

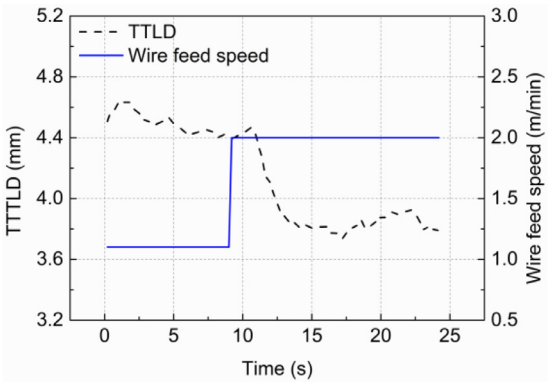

Fig. 5. Transient step response of TTLD to wire feed speed.

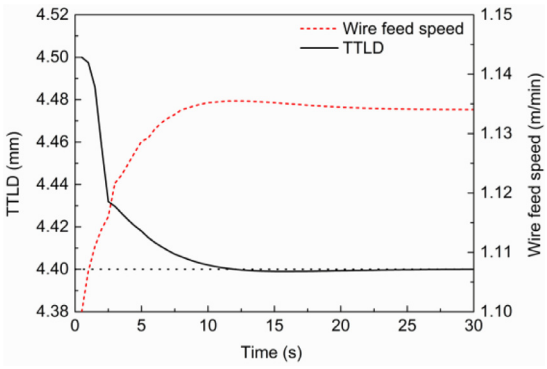

Fig. 7. Simulation curves based on the dynamic characteristics in GTA-based additive manufacturing.

solidified layers. In this case, no other spectra from the arc can pass through the narrow-band filter other than the wavelength of 685 nm. The acquired image was composed of only the intensity of 685 nm and the continuum radiation lights near this wavelength.

Since the visual sensor is fixed on the GTA torch, the position of the tungsten tip in the image is invariable. Then the key issue for measuring the TTLD is to determine the edge of the top layer surface. Captured images need to be treated by the computer image processing for extracting features of the top layer surface. Fig. 4 presents the procedure of image processing for the TTLD in GTA-based additive manufacturing. As can be seen, the original image was treated by many image processing algorithms, i.e. setting a small window for saving computational time, Gaussian filter for removing noises, Sobel operator for top edge detection, and Hough transformation for top edge fitting. The image processing algorithms were programmed with C++ language in Microsoft visual studio 2010 environment. After extracting the row coordinate of the top surface, the TTLD value can be calculated by row deviations between the tungsten tip and the top layer edge.

The next step is to calibrate the visual sensor for obtaining the pixel number versus the real value in the world coordinate system. In this study, a template with a series of 1×1 mm^2 grids was placed in the *YOZ*-plane shown in Fig. 3. Then, the spatial resolution in the *Z*-axis is calculated as 0.0155 mm/pixel.

3. Process modeling and controller design

3.1. Process identification

This research aims at increasing the process stability in GTA-based additive manufacturing, which is achieved by designing a closed-loop controller to regulate the process variables during the fabrication process. The control output is the TTLD value, and the wire feed speed having a strong affection on the height geometry is selected as the control input. In GTA-based process, it is believed that the wire feed speed has a major action on the layer height than the arc current [16], and the travel speed is not suitable to be regulated in real time in robotic motion. Although adjusting the wire feed speed can slightly affect the geometry of the layer width, this impact is not considered when fabricating multi-layer single-pass walls. In general, a control system includes modeling the dynamic features of a controlled object and designing an optimal controller. The dynamic characteristics can be identified by motivating the dynamic changes in the process. To design an excellent controller, the premise is to obtain the dynamic correlation between the controlling and controlled variables.

It is believed that the dynamic characteristics of the arc-based process can be approximated with a first-order transfer function [35]. By conducting step response experiments, the transfer function can be calculated based on analyzing the step response curves. Generally, a first-order transfer function is expressed as:

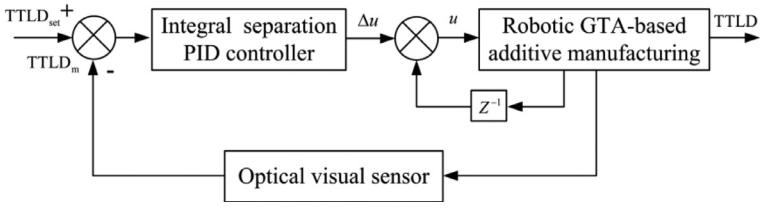

Fig. 6. Schematic diagram of the integral separation PID control system for GTA-based additive manufacturing.

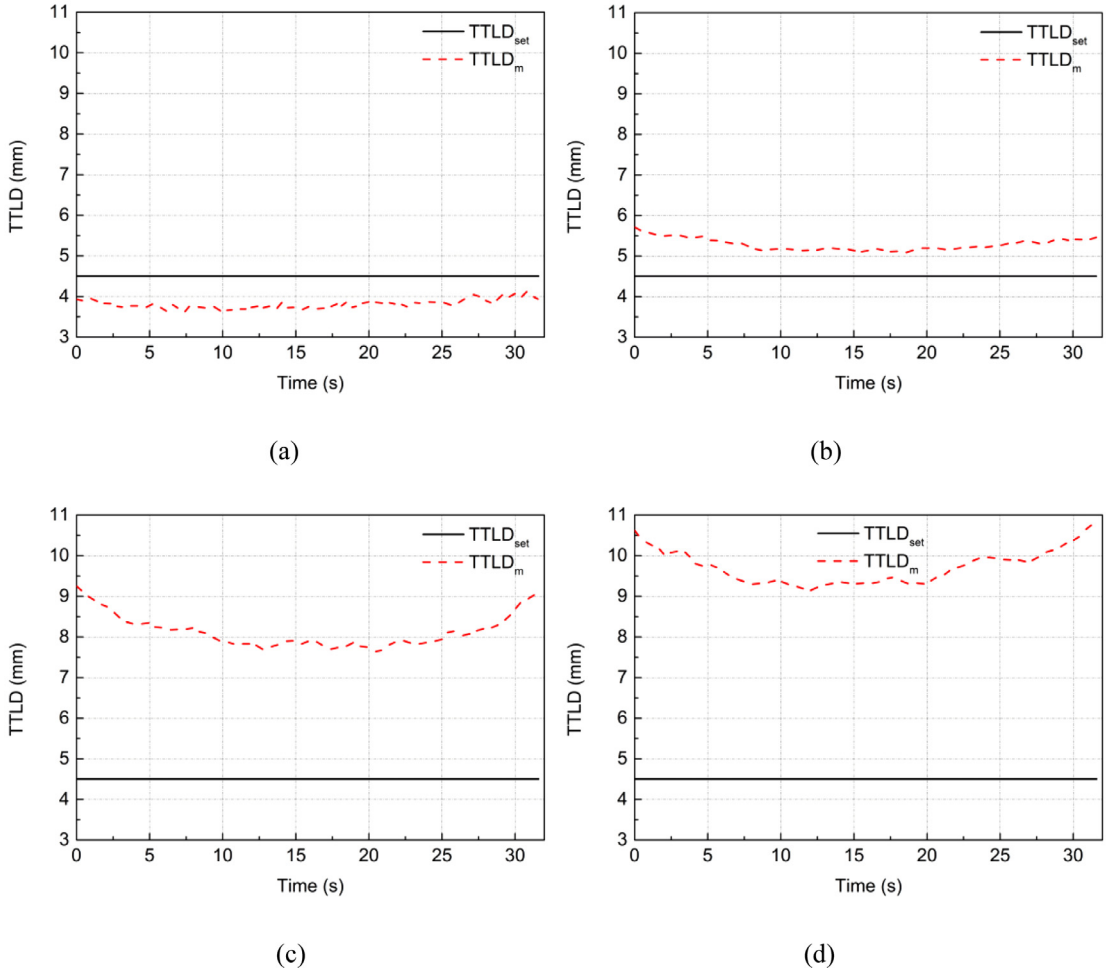

Fig. 8. TTLD measurements of different layers for the 18-layerd wall deposited in GTA-based additive manufacturing. (a) 3rd layer. (b) 7th layer. (c) 15th layer. (d) 18th layer.

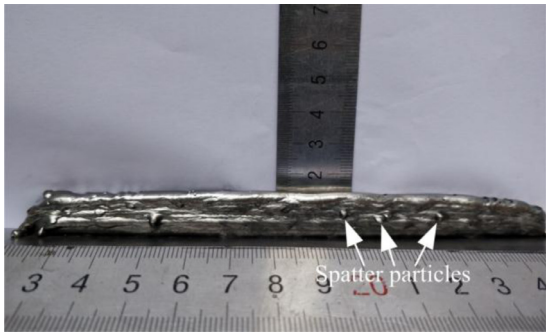

Fig. 9. Photo of the 18-layered wall deposited in open-loop control test.

$$P(s) = \frac{K}{1 + T_s} e^{-\tau s} \tag{1}$$

where K is the gain coefficient, τ is the time lag constant, and T_s is the time constant.

A step response test was designed to identify the process model. Firstly, a four-layer single-pass part with a length of 140 mm was deposited on the substrate, the wire feed speed was 1.1 m/min and other process variables are described in Section 2.1. The step response test was carried out in the fifth layer. This is because the layer geometries of the first four layers are unstable owing to the thermal role of the substrate [36]. During the deposition of the fifth layer, as the GTA torch moved to the midpoint of the fifth layer, the wire feed speed was transiently changed from 1.1 to 2.0 m/min. The variable TTLD was also detected, as shown in Fig. 5. On the basis of the step response curves in Fig. 5, the transfer function of the model can be calculated using the system identification toolbox in MATLAB software. In this research, the parameters of the transfer function are: $K = -0.75$, $T_s = 1.18$, and $\tau = 2$.

3.2. Closed-loop controller design

GTA-based additive manufacturing is a fabrication process in a layer by layer manner and is disturbed by a series of process variables, showing more sophisticated than the common GTA welding process. Therefore, a closed-loop controller is essential to be designed to increase the process stability. An adaptive PID controller, which is extensively used in the industrial field for the reason that it's reliable and can be easily regulated, is employed for on-line control of GTA-based additive manufacturing. A continuous PID controller algorithm is given as:

$$u(t) = \left[e(t) \int_0^t e(t)dt \frac{de(t)}{dt} \right] \begin{bmatrix} k_p \\ k_p/T_I \\ k_p T_D \end{bmatrix} \tag{2}$$

where $u(t)$ is the controlling variable, k_p is the proportion coefficient, T_I is the integral coefficient, T_D is the derivative factor, t is the time, and $e(t)$ is the deviation between the given value $r(t)$ and the actual output value $y(t)$, which is given as:

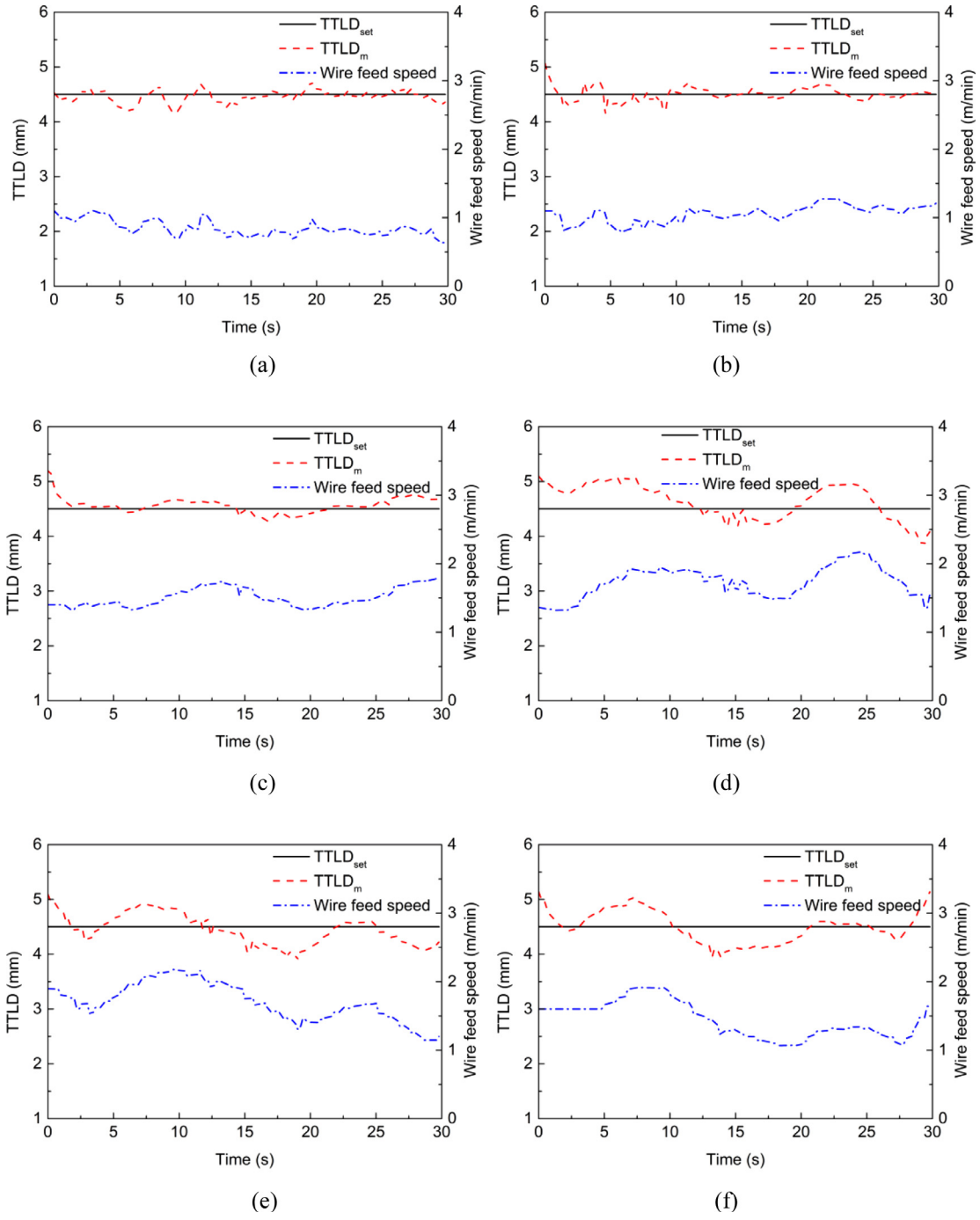

Fig. 10. Closed-loop control of TTLD in various layers for the 25-layered wall fabricated in GTA-based additive manufacturing. (a) 2nd layer. (b) 4th layer. (c) 6th layer. (d) 17th layer. (e) 21th layer. (f) 25th layer.

$$e(t) = r(t) - y(t) \tag{3}$$

Generally, increments of controlling variables are widely utilized in the discrete measuring and control system. The continuous PID controller in Eq. (2) can be dispersed into an incremental controller.

$$\Delta u(t) = k_p Y(1) + k_i Y(2) + k_d Y(3) \tag{4}$$

where $\Delta u(t)$ is the increment of the controlling variable, $k_i = k_p/T_I$, and $k_d = k_p T_D$. $Y(1)$, $Y(2)$, and $Y(3)$ are given as:

$$Y(1) = e(t) - e(t-1) Y(2) = e(t) Y(3) = e(t) - 2e(t-1) + e(t-2) \tag{5}$$

Although the integral effect in the conventional PID controller can eliminate the static error of the automatic control system, it is also able to produce the vibration and overshoot of the process. To prevent the overshoot in the conventional PID controller, an integral separation factor is added to the controller for GTA-based additive manufacturing. The basic principle of the integral separation is that the integral effect is cancelled when generating a large $e(t)$ and is introduced as the detected value is close to the given value. Thus, Eq. (4) can be transformed as:

$$\Delta u(t) = k_p Y(1) + \beta k_i Y(2) + k_d Y(3) \tag{6}$$

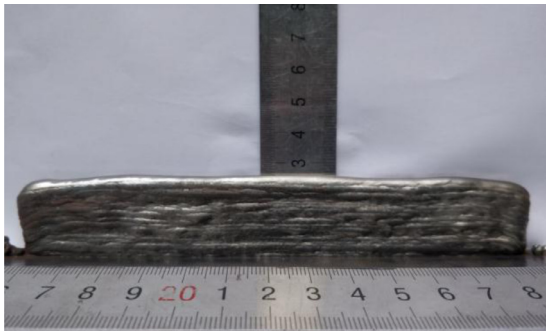

Fig. 11. Photo of the 25-layered wall fabricated in closed-loop control experiment.

$$\beta = \begin{cases} a_1 & |e(t)| \le M_1 \\ a_2 & M_1 < |e(t)| \le M_2 \\ a_3 & M_2 < |e(t)| \le M_3 \\ a_4 & |e(t)| > M_3 \end{cases} \quad (7)$$

where M_1, M_2, M_3, and M_4 are thresholds of the deviation between the setting and detected values, and a_1, a_2, a_3, and a_4 are integral-separation coefficients.

Fig. 6 presents the schematic diagram of the integral separation PID controller for GTA-based additive manufacturing. $TTLD_{set}$ is the predefined height, $TTLD_m$ is the height extracted by processing of images captured via the visual sensing system, and Δu is the increment of the wire feed speed. The deviation between the predefined and measured heights is taken as the input of the controller. Then, the increment of the wire feed speed can be calculated by the integral separation PID controller. The visual detection and feedback control are repeated during the whole deposition process.

4. Results and discussion

Before applying the controller to actual GTA-based additive manufacturing, the coefficients in Eq. (6) must be adjusted to obtain an excellent performance of the closed-loop controller. However, the parameter adjustment during the experimental process wastes lots of time and materials. Based on the dynamic model obtained in Section 3.1, the controller simulation was performed using MALTAB language, and the simulation results are shown in Fig. 7. The TTLD is the controlled variable, and the wire feed speed is the controlling variable. The initial wire feed speed and TTLD are 1.1 m/min and 4.5 mm, respectively. At $t = 0$ s, the given TTLD is set at 4.4 mm, and the wire feed speed gradually increases to 1.134 m/min. As shown in Fig. 7, the setting time is about 9.8 s.

After performing the controller simulation, the performance of the integral separation PID controller should be tested through depositing multi-layer single-pass parts. To prove the effectiveness of the proposed controller, two kinds of experiments were carried out, i.e. open-loop and closed-loop control tests. The initial distance between the tungsten tip and the substrate surface was set at 5.5 mm. Other process parameters are given in Section 2. When one layer was completed, the GTA torch was raised by a constant layer height of 1.0 mm. In the open-loop control experiment, an 18-layered wall was deposited and the wire feed speed of 1.1 m/min was kept constant during the fabrication process. In the closed-loop control test, a 25-layered wall was built, and the wire feed speed was adjusted by the designed controller to keep the TTLD stable. It is noted that the initial wire feed speed was 1.1 m/min for the first five layers. Considering that the heat conduction condition having a significant affection on the layer height becomes worse with the proceeding of the deposition process, setting a suitable initial wire feed speed can increase the regulation speed of the controller for rapidly achieving the steady value. In this research, after depositing the first five layers, the initial wire feed speed was calculated based on the average value of the sampled wire feed speed of the previous layer. This was achieved by reading average value from the human-machine interface.

Fig. 8 shows the detected TTLD values of different layers in the open-loop control test. The sampling period of the control system is 0.25 s. The black solid line is the given TTLD, and the red dash line is the detected TTLD. The detections of both ends of the thin-walled parts, such as arc starting and extinguishing points, are not conducted. As seen in Fig. 8, the measured TTLD increases gradually with the increasing deposition height. For instance, the average of the TTLD values in Fig. 8(a) is 3.81 mm which is less than the given TTLD, and that in Fig. 8(d) is approximately 9.71 mm. It is believed that the TTLD ranging from 3 to 7 mm can keep the stability in GTA process. As shown in Fig. 8(c) and (d), the values on both ends of the measured TTLD curves are larger in comparison to the middle regions. The reason is that molten pool close to both ends of the thin-wall is unstable due to the effect of the arc starting and extinguishing points. It is indicated that the deposition heights on both ends of the thin-walled parts are lower than those in the middle region. Fig. 9 shows the macrophotograph of the 18-layered wall. Many deposition spatters can be observed on the side face of the component. It is demonstrated that droplets present globular transfer due to the too large TTLD during the deposition process, resulting in the instability in GTA-based additive manufacturing.

Fig. 10 displays the control results of the TTLD in different layers for a 25-layered wall when the integral separation PID controller is employed. The sampling and control periods are set at 0.25 and 0.5 s,

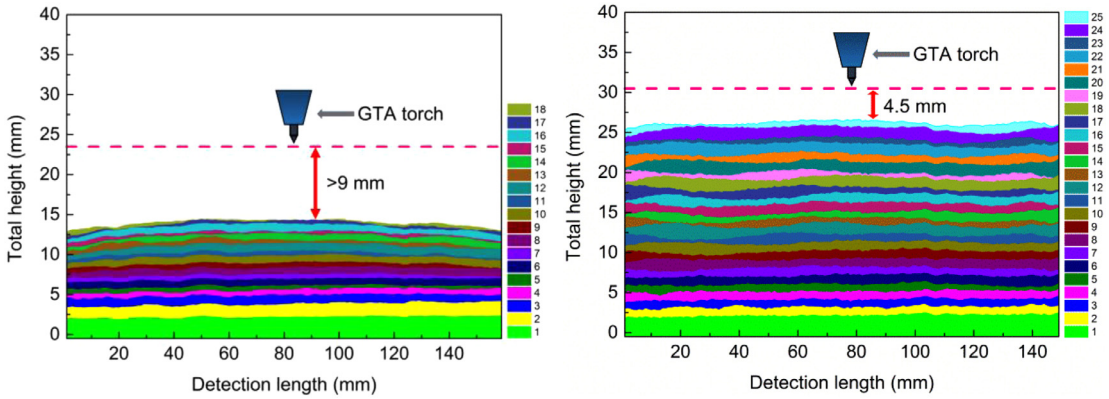

Fig. 12. Position relationship between the GTA torch and the total height of the thin-walled parts. (a) 18-layered wall. (b) 25-layered wall.

respectively. The black solid and red dash lines are the given and detected TTLD values, respectively, and the blue dash dot line is the adjusted wire feed speed. As can be shown in Fig. 10, the measured TTLD curves fluctuate around the setting TTLD value. It is demonstrated that the proposed controller can keep the fabrication process stable. The maximum deviations between the set point and the detected TTLD values in Fig. 10 are mostly limited to 0.4 mm. The fluctuations of the TTLD in Fig. 10(a)–(c) are small. As shown in Fig. 10(d)–(f), although the measured TTLD values fluctuate around the given value, the fluctuation ranges of the detected values are large. The mean square errors of the TTLD in Fig. 10 are 0.118, 0.109, 0.119, 0.343, 0.276, and 0.296, respectively. This means that poor flatness can be observed on the top surface of the component, as presented in Fig. 11.

The passive vision sensor is employed to detect the solidified layer surface which is close to the molten pool tail. Thus, a certain time lag inevitably exists in the detection system. Moreover, the closed-loop control for height control is a feedback control method. The height homogeneity of the previous layer has a strong influence on the height geometry of the current layer. To further increase the control accuracy of the TTLD values, a feedforward controller will be introduced to detect the height geometry of the previous layers, and the deviation will be considered into the feedback control system.

In recent years, layer height prediction algorithms have been studied in many references, such as modelling between layer geometry and process parameters [37], establishing overlapping models for thick walls [38], prediction of layer thickness for thin-walled parts [1]. The predicted layer height is regarded as the slicing height of a three-dimensional model. However, the predicted layer height is a theoretical value without considering disturbances in arc-based additive manufacturing. Owing to various disturbances discussed in Section 1, especially the effect of heat accumulation at different layers, the actually deposited layer height is not always identical with the predicted value. By applying the sensing and closed-loop control technique to slightly adjust the process parameters, the fabricated layer height can be indirectly controlled to the torch step height.

In general, the layer height of the nth layer is calculated as:

$$h_n = h + TTLD_{n-1} - TTLD_n \tag{8}$$

where h is the raised height of the GTA torch for each layer, $TTLD_{n\text{-}1}$ and $TTLD_n$ are the tungsten to top layer distances in the $(n-1)$th and nth layer, respectively. The total height of the wall after depositing the nth layer can be expressed as:

$$H_n = TTLD_0 + nh - TTLD_n \tag{9}$$

where $TTLD_0$ is the initial distance between the tungsten tip to the substrate surface.

Fig. 12 presents the position relationship between the GTA torch and the total height of the thin-walled parts fabricated under open-loop and closed-loop control tests. As seen in Fig. 12(a), the length between the tungsten and the top layer surface exceeds 9 mm, decreasing the process stability in GTA-based additive manufacturing. As displayed in Fig. 12(b), the tungsten to the top surface distance is approximately 4.5 mm. Nevertheless, with the increasing deposition height, the height curves for some layers fluctuate apparently. In future study, the stability of the height geometry needs to be further improved.

It is noted that the designed passive vision sensor in this study is well suitable for multi-layer single-pass parts and is hard to be applied to multi-layer multi-pass components. The reason is that the visual sensor is fixed opposite the GTA torch, as presented in Fig. 3. When fabricating multi-layer multi-pass parts, the height information of the subsequent overlapping beads in the same layer cannot be easily detected due to the vision barrier of the previously deposited beads. Moreover, as more overlapping beads in a layer are deposited, a collision may be produced between the visual sensor and the previously deposited beads. In fact, the height detection of multi-layer multi-pass parts is a difficult issue needed to be solved. In future work, a virtual sensing system based on the arc voltage sensor is expected to increase the process stability for multi-layer multi-pass components built in GTA-based additive manufacturing.

5. Conclusions

This research aims at increasing process stability in GTA-based additive manufacturing through optical measurement and feedback control. The effectiveness of the proposed approach is validated through deposition of thin-walled components. The main conclusions are listed below.

(1) The process stability in GTA-based additive manufacturing is represented by the tungsten to top layer distance. A passive vision sensor, including a camera, a lens, a dimmer glass, and a narrow-band filter, was designed to measure the TTLD.
(2) Image processing algorithms were applied to extract the top surface of the layers in captured images, such as Gaussian filter to remove noise, edge detection to determine layer edge, threshold segmentation to calculate optimal threshold, and Hough transformation for edge fitting.
(3) An integral separation PID controller was used to adjust the wire feed speed. The transfer function model of the process was established by conducting the step response test of the wire feed speed. The optimal process parameters of the controller were determined by controller simulation programmed using MATLAB language.
(4) Comparison tests including the constant parameters and feedback control were carried out. In the feedback control test, the controlled variable was TTLD and the controlling signal was the wire feed speed. The controller ensures consistent TTLD value during the deposition process, and the maximum deviation between the given value and the detected TTLD can be mostly limited to 0.4 mm, proving the capability of the feedback controller to increase the process stability and to prevent the risk for stubbing and large droplet transfer.

Acknowledgments

This work was funded by National Natural Science Foundation of China, no. 61573293 and no. 51505394, Sichuan Science and Technology Program, no. 2019YFG0354, and the Fundamental Research Funds for the Central Universities, no. 2682019CX12.

Supplementary materials

Supplementary material associated with this article can be found, in the online version, at doi:10.1016/j.rcim.2019.05.012.

References

[1] J.S. Panchagnula, S. Simhambhatla, Manufacture of complex thin-walled metallic objects using weld-deposition based additive manufacturing, Robot. Comput.-Integr. Manuf. 49 (2018) 194–203.
[2] S.W. Williams, F. Martina, A.C. Addison, J. Ding, G. Pardal, P. Colegrove, Wire + arc additive manufacturing, Mater. Sci. Technol. 32 (2016) 641–647.
[3] D.Q. Yang, G. Wang, G.J. Zhang, Thermal analysis for single-pass multi-layer GMAW based additive manufacturing using infrared thermography, J. Mater. Process. Technol. 244 (2017) 215–244.
[4] A. Horgar, H. Fostervoll, B. Nyhus, X. Ren, M. Eriksson, O.M. Akselsen, Additive manufacturing using WAAM with AA5183 wire, J. Mater. Process. Technol. 259 (2018) 68–74.
[5] F. Hejripour, D.T. Valentine, D.K. Aidun, Study of mass transport in cold wire deposition for wire arc additive manufacturing, Int. J. Heat Mass Transf. 125 (2018) 471–484.
[6] C. Shen, Z.X. Pan, D. Cuiuri, D.H. Ding, H.J. Li, Influences of deposition current and interpass temperature to the Fe_3Al-based iron aluminide fabricated using wire-arc additive manufacturing process, Int. J. Adv. Manuf. Technol. 88 (5-8) (2017) 2009–2018.
[7] P. Kazanas, P. Deherkar, P. Almeida, H. Lockett, S. Williams, Fabrication of geometrical features using wire and arc additive manufacture, Proc. Inst. Mech. Eng. B

226 (B6) (2012) 1042–1051.
[8] D.H. Ding, Z.X. Pan, D. Cuiuri, H.J. Li, A practical path planning methodology for wire and arc additive manufacturing of thin-walled structures, Rob. Comput. Integr. Manuf. 34 (2015) 8–19.
[9] D.H. Ding, Z.X. Pan, D. Cuiuri, H.J. Li, N. Larkin, S. van Duin, Automatic multi-direction slicing algorithms for wire based additive manufacturing, Rob. Comput. Integr. Manuf. 37 (2016) 139–150.
[10] P.A. Colegrove, H.E. Coules, J. Fairman, F. Martina, T. Kashoob, H. Mamash, L.D. Cozzolino, Microstructure and residual stress improvement in wire and arc additively manufactured parts through high-pressure rolling, J. Mater. Process. Technol. 213 (2013) 1782–1791.
[11] Y.H. Fu, H.O. Zhang, G.L.Wang, H.F. Wang, Investigation of mechanical properties for hybrid deposition and microrolling of bainite steel, J. Mater. Process. Technol. 250 (2017) 220–227.
[12] J. Xiong, R. Li, Y.Y. Lei, H. Chen, Heat propagation of circular thin-walled parts fabricated in additive manufacturing using gas metal arc welding, J. Mater. Process. Technol. 251 (2018) 12–19.
[13] H.H. Zhao, G.J. Zhang, Z.Q. Yin, L. Wu, Three-dimensional finite element analysis of thermal stress in single-pass multi-layer weld-based rapid prototyping, J. Mater. Process. Technol. 212 (2012) 276–285.
[14] Y.J. Li, J. Xiong, Z.Q. Yin, Molten pool stability of thin-wall parts in robotic GMA-based additive manufacturing with various position depositions, Rob. Comput. Integr. Manuf. 56 (2019) 1–11.
[15] B. Baufeld, O.V.D. Biest, R. Gault, Additive manufacturing of Ti-6Al-4V components by shaped metal deposition: microstructure and mechanical properties, Mater. Des. 31 (2010) S106–S111.
[16] F. Bonaccorso, L. Cantelli, G. Muscato, An arc welding robot control for a shaped metal deposition plant: modular software interface and sensors, IEEE Trans. Ind. Electron. 58 (8) (2011) 3126–3132.
[17] Y.Y. Ding, W. Huang, R. Kovacevic, An on-line shape-matching weld seam tracking system, Rob. Comput. Integr. Manuf. 42 (2016) 103–112.
[18] Y.L. Xu, G. Fang, N. Lv, S.B. Chen, J.J. Zou, Computer vision technology for seam tracking in robotic GTAW and GMAW, Rob. Comput. Integr. Manuf. 32 (2015) 25–36.
[19] A. Heralic, A.K. Christiansson, M. Ottosson, B. Lennartson, Increased stability in laser metal wire deposition through feedback from optical measurements, Opt. Lasers Eng. 48 (2010) 478–485.
[20] A. Heralic, A.K. Christiansson, B. Lennartson, Height control of laser metal-wire deposition based on iterative learning control and 3D scanning, Opt. Lasers Eng. 50 (2012) 1230–1241.
[21] L. Tang, R.G. Landers, Layer-to-layer height control for laser metal deposition process, J. Manuf. Sci. Eng. 133 (2011) 021009.
[22] Y.S. He, Y.L. Xu, Y.X. Chen, H.B. Chen, S.B. Chen, Weld seam profile detection and feature point extraction for multi-pass route planning based on visual attention model, Robot. Comput.-Integr. Manuf. 37 (2016) 251–261.
[23] J. Xiong, S.Y. Zou, Active vision sensing and feedback control of back penetration for thin sheet aluminum alloy in pulsed MIG suspension welding, J. Process. Control 77 (2019) 89–96.
[24] M. Luo, Y.C. Shin, Vision-based weld pool boundary extraction and width measurement during keyhole fiber laser welding, Opt. Lasers Eng. 64 (2015) 59–70.
[25] G. Saeed, Y.M. Zhang, Weld pool surface depth measurement using a calibrated camera and structured light, Measure. Sci. Technol. 18 (2007) 2570–2578.
[26] Y.K. Liu, Y.M. Zhang, Control of 3D weld pool surface, Control Eng. Pract. 21 (2013) 1469–1480.
[27] C. Doumanidis, Y.M. Kwak, Multivariable adaptive control of the bead profile geometry in gas metal arc welding with thermal scanning, Int. J. Press.Vessels Pip. 79 (2002) 251–262.
[28] T.F. Comas, C.L. Diao, J.L. Ding, S. Williams, Y.F. Zhao, A passive imaging system for geometry measurement for the plasma arc welding process, IEEE Trans. Ind. Electron. 64 (2017) 7201–7209.
[29] J. Xiong, G.J. Zhang, Online measurement of bead geometry in GMAW-based additive manufacturing using passive vision, Measure. Sci. Technol. 24 (11) (2013) 115103.
[30] J. Xiong, G.J. Zhang, Z.L. Qiu, Y.Z. Li, Vision-sensing and bead width control of a single-bead multi-layer part: material and energy savings in GMAW-based rapid manufacturing, J. Clean Prod. 41 (2013) 82–88.
[31] J. Xiong, G.J. Zhang, Adaptive control of deposited height in GMAW-based layer additive manufacturing, J. Mater. Process. Technol. 214 (2014) 962–968.
[32] H. Wang, R. Kovacevic, Rapid prototyping based on variable polarity gas tungsten arc welding for a 5356 aluminium alloy, Proc. Inst. Mech. Eng. Part B 215 (2001) 1519–1527.
[33] H. Wang, W. Jiang, J. Ouyang, R. Kovacevic, Rapid prototyping of 4043 Al-alloy parts by VP-GTAW, J. Mater. Process. Technol. 148 (1) (2004) 93–102.
[34] J. Xiong, Y.Y. Lei, H. Chen, G.J. Zhang, Fabrication of inclined thin-walled parts in multi-layer single-pass GMAW-based additive manufacturing with flat position deposition, J. Mater. Process. Technol. 240 (2017) 397–403.
[35] S.B. Chen, Y.J. Lou, L. Wu, D.B. Zhao, Intelligent methodology for measuring, modeling, control of dynamic process during pulsed GTAW: Part I bead-on-plate welding, Weld. J. 79 (6) (2000) 151–163.
[36] F. Martina, J. Mehnen, S.W. Williams, P. Colegrove, F. Wang, Investigation of the benefits of plasma deposition for the additive layer manufacture of Ti-6Al-4V, J. Mater. Process. Technol. 212 (2012) 1377–1386.
[37] J. Xiong, G.J. Zhang, J.W. Hu, L. Wu, Bead geometry prediction for robotic GMAW-based rapid manufacturing through a neural network and a second-order regression analysis, J. Intell. Manuf. 25 (1) (2014) 157–163.
[38] W. Aiyiti, W.H. Zhao, B.H. Lu, Y.P. Tang, Investigation of the overlapping parameters of MPAW-based rapid prototyping, Rapid. Prototyp. J. 12 (3) (2006) 165–172.